

Supporting Information

PhotocARRIER Tunneling Triggering CO₂ Photocatalysis

Xian Yan^a, Meng Yuan^a, Ya-Long Yuan^a, Peng Su^a, Qing Chen^a, Fang-Xing Xiao^{*a,b}

a. College of Materials Science and Engineering, Fuzhou University, New Campus, Fujian Province,
350108, China.

b. State Key Laboratory of Structural Chemistry, Fujian Institute of Research on the Structure of Matter,
Chinese Academy of Sciences, Fuzhou, Fujian 350002, PR China

E-mail: fxxiao@fzu.edu.cn

Table of Contents

Experimental section	S1
Figure S1. Zeta potentials (ξ) of CdS, C@P1 and Ag@citrateNCs.....	S6
Figure S2. Raman of CdS, C@P1 and C@P1@A1 heterostructure.....	S7
Figure S3. UV-vis absorption spectrum of PAH aqueous solution.....	S8
Figure S4. UV-vis absorption spectrum of citrate.....	S9
Figure S5. UV-vis absorption spectrum of Ag@citrate aqueous solution.....	S10
Figure S6. HRTEM image of Ag@citrate NCs and size distribution histogram.....	S11
Figure S7. N ₂ adsorption-desorption isotherms of CdS and C@P1/A1 heterostructure.....	S12
Figure S8. EDX images of (a) C@P1 and (b) C@P1@A1.....	S13
Figure S9. FESEM and EDS images of C@P1/A1 heterostructure.....	S14
Figure S10. CV curves of PAH and EIS Nyquist plots of CdS, C@P1, C@P5 and C@P10.....	S15
Figure S11. FESEM and EDS images of C@P1/A1 after cyclic photoreduction reactions.....	S16
Figure S12. XRD patterns of C@P1/A1 (I) before and (II) after cyclic photoreduction reactions.....	S17
Figure S13. FTIR spectra of C@P15@Au7 (I) before and (II) after cyclic photoreduction reactions.....	S18
Figure S14. Raman of C@P1@A1 (I) before and (II) after cyclic photoreduction reactions.....	S19
Figure S15. XPS spectra of C@P1/A1 (II) before and (III) after cyclic photoreduction reactions.....	S20
Figure S16. XRD patterns of C@P1@S and C@P1@S/A1.....	S21
Figure S17. FESEM and elemental mapping images of C@P1@S.....	S22
Figure S18. FESEM and elemental mapping images of C@P1@S/A1.....	S23
Figure S19. TGA curve of C/A1 and C@P/A1.....	S24
Figure S20. FESEM images of (a) C@P1/A1 and (b) C@P1/A1-700 °C.....	S25
Figure S21. Photoreduction nitroaromatics of C@P1/A1, C@P1/A1-700 °C and C@P1@S/A1.....	S26
Figure S22. Mott-Schottky plots of CdS with energy band.....	S27
Table S1. Peak position with corresponding functional group.....	S28
Table S2. Chemical bond species vs. B.E. for CdS and C@P1/A1.....	S29
Table S3. Summary of specific surface area, pore volume and pore size of CdS and C@P1/A1.....	S30
Table S4. Fitted EIS results of different samples based on the equivalent circuit.....	S31
Table S5. C/A1 and C@P1/A1 selective photoreduction of aromatic nitro compounds.....	S32
Table S6. C@P1/S@A1 and C@P1/A1-700 °C selective photoreduction of aromatic nitro compounds.....	S33
References	S34

1. Experimental section

1.1 Materials

Cadmium acetate dihydrate ($C_4H_6CdO_4 \cdot 2H_2O$), Thiourea (CH_4N_2S), Hydrofluoric acid (HF 40 wt%), sodium borohydride ($NaBH_4$), silver nitrate ($AgNO_3$), sodium citrate, Poly (diallyl-dimethylammonium chloride) (PDDA) ($M_w = 200000$ g/mol), poly (allylamine hydrochloride) (PAH, average $M_w=17.5$ kDa), tetraethyl orthosilicate (TEOS), methanol (CH_4O), ethylene glycol ($C_2H_6O_2$), lactic acid ($C_3H_6O_3$), sodium sulfide nonahydrate ($Na_2S \cdot 9H_2O$), sodium sulfite (Na_2SO_3), sodium sulfate (Na_2SO_4), triethanolamine (TEOA), acetonitrile (C_2H_3N), Ammonium formate (CH_5NO_2), 4-nitroaniline (4-NA), 3-nitroaniline (3-NA), 2-nitrophenol (2-NP), 4-nitroanisole, 4-nitrotoluene nitrobenzene, o-nitroacetophenone and deionized water (DI H_2O , Millipore, 18.2 M Ω cm resistivity) are used. All the materials are of analytical grade and used as received without further purification.

1.2 Preparation of CdS nano-leaves

Specifically, 5 mmol $C_4H_6CdO_4 \cdot 2H_2O$, 6 mmol CH_4N_2S , 0.805 mL HF (40 wt%) and 79.2 mL of deionized water were added into a 100 mL Teflon autoclave to 80% volume. After stirring at room temperature for 1.5 h, the autoclave was sealed and maintained at 200 °C for 20 h, and then air cooled to room temperature. The precipitate obtained was filtered and washed several times with DI H_2O and absolute ethanol, and then dried in vacuum at 60 °C for 8 h.¹

1.3 Preparation of positively charged CdS@PAH (C@P)

Pre-selected 0.2 g CdS as the substrate material and weighed PAH according to its mass ratio, and then dispersed the two samples into 20 mL DI H_2O and stirred for 1 h. Mixtures were labeled as C@P-X (X : 0.5, 1, 2, 5 and 10) after centrifugal collection, and then dried in vacuum at 60 °C for 8 h.

1.4 Preparation of positively charged Ag NCs (Ag@citrate NCs)

Citrate-stabilized Ag NCs were synthesized based on an aqueous synthesis method reported previously.² Typically, 100 mL of a 1 mM aqueous AgNO₃ solution was mixed with 8 mL of a 40 mM aqueous sodium citrate solution used as stabilizer. Subsequently, A total of 2 mL of a 112 mM aqueous NaBH₄ solution was then added dropwise under vigorous stirring (2500 rpm) at ambient temperature, immediately yielding a yellowish brown Ag hydrosol. The Ag hydrosol was stocked in a refrigerator at 4 °C and aged for 24 h to decompose the residual NaBH₄ before it was used in subsequent steps.

1.5 Preparation of CdS/Ag@citrate NCs (C/A) and CdS@PAH/Ag@citrate NCs (C@P/A) heterostructures

The construction of C@P/A heterostructure was achieved by electrostatic self-assembly using C@P1 as the substrate and Ag@citrate NCs as the anchoring block. Specifically, Ag@citrate NCs aqueous solution was added dropwise to the 0.1 g C@P1 aqueous dispersion according to the mass ratio under vigorous stirring. After mixing for 2 h, the mixtures were centrifuged and labeled as C@P1/A-X (X: 0.5, 1, 2, 3 and 5), and then dried in vacuum at 60 °C for 8 h.

As a control sample, C/A1 was prepared in the same way as described above.

1.6 Preparation of CdS@PAH1@SiO₂ (C@P1@S) and CdS@PAH1@SiO₂/Ag@citrate 1 (C@P1@S/A1) heterostructures

50 mg of C@P1 was added to 10 mL aqueous solution, then 50 mL ethanol, 2 mL ammonium hydroxide and 1.6 mL TEOS were added successively. After stirring for 1 hour, the mixture was centrifuged and the resulting SiO₂-coated C@P1 was thoroughly washed with ethanol and deionized water and dried in air. Increase the amount of DI H₂O, ethanol, ammonium hydroxide and TEOS by 2.5 times to get CdS@PAH1@SiO₂ (C@P1@S).

The preparation process of C@P1@S/A1 is the same as that of C@P1/A1.

1.7 Characterization

The crystal structure was determined by X-ray diffraction (XRD, Miniflex600). Morphologies were visualized by field emission scanning electron microscopy (FESEM, Supra55, Carl Zeiss) equipped with energy-dispersive spectroscopy (EDS) and transmission electron microscopy (TEM, Tecnai G2 F20). Fourier transform infrared (FTIR) spectra were recorded on an infrared spectrophotometer (TJ270-30A). Raman spectra were collected with a Raman spectrometer (Dxr-2xi, Thermo Scientific, America). UV-visible diffuse reflectance spectra (DRS) were measured on Cary50 (Varian, America) with the reflectance background from 200 to 800 nm. X-ray photoelectron spectra (XPS) were recorded on a photoelectron spectrometer (ESCALAB 250, Thermo Scientific, America), and the binding energy (BE) of the elements were calibrated by the BE of C 1s (284.80 eV). Zeta potential (ξ) measurements were performed by dynamic light scattering analysis (Zeta sizer Nano ZS-90). Time-resolved photoluminescence (TRPL) spectra were measured on a FLS 920 fluorescence lifetime spectrophotometer (Edinburgh, Instruments, UK). The photoluminescence (PL) spectra were probed on a Varian Cary Eclipse spectrophotometer. Brunauer-Emmett-Teller (BET) specific surface area and N₂ adsorption experiments were performed on ASAP 2460.

1.8 Photocatalytic CO₂ reduction

Specifically, 10 mg of the catalyst was dispersed in mixed solution (DI H₂O (2 mL), triethanolamine (TEOA, 3 mL) and C₂H₃N (5 mL) and stirred (1000 rpm) throughout the reaction to ensure that the catalyst was in suspension throughout the experiment. The reaction system was evacuated to eliminate other impurity gases. Then, high purity CO₂ was introduced to the reaction system with a partial pressure of 1 atm. After light irradiation ($\lambda > 420$ nm) for 2 h, the generated products were sampled and quantified by gas chromatograph (SHIMADZU, GC-2014C). The stability of the cycle was tested as follows. After the first run, the

photocatalytic system was again subjected to complete degassing, introduction of CO₂, and replenishment of acetonitrile without separating the catalyst, and then the next set of light irradiation tests were performed.

1.9 Photoreduction performances

Specifically, 10 mg of catalyst and 40 mg of ammonium formate (NH₄HCO₂) were mixed with 40 mL of 4-NA aqueous solution (30 ppm) in a glass reactor under N₂ bubbling. After vigorously stirring in dark for 30 min to reach the adsorption-desorption equilibrium, the glass vessel was irradiated by visible light ($\lambda > 420$ nm). 2 mL of the sample solution was collected at regular time intervals (0, 20, 40, 60, 80 and 100 s), centrifuged (12000 rpm), and the supernatant was analyzed by a UV-vis absorption spectrophotometer. Photoreduction of other aromatic nitro compounds were also carried out under the same conditions. Photoactivities of samples was defined by following formula.

$$\text{Conversion (\%)} = \frac{C_0 - C}{C_0} \times 100 \quad (1)$$

2.0 Photoelectrochemical (PEC) measurements

PEC measurements were carried out on an electrochemical workstation (CHI660E, CHI Shanghai, Inc.) with conventional three-electrode system and 0.5 M Na₂SO₄ aqueous solution (pH = 6.69) was utilized as the electrolyte. The three-electrode system is composed of Pt foil (1 cm × 1 cm) as the counter electrode, Ag/AgCl electrode as the reference electrode and working electrodes. The working electrodes were prepared on fluorine-doped tin oxide (FTO) glass that was cleaned by sonication in DI H₂O and ethanol for 30 min and dried at 60 °C in an oven. Specifically, 15 mg of the sample was dispersed in 3 mL of ethanol by sonication to get slurry which was spread onto the pretreated FTO glass. After air drying, the Scotch tape was unstuck and the uncoated part of the electrode was isolated with nail polish. The exposed area of the working electrode was 1 cm². Finally, the working electrode was vertically dipped into the electrolyte and irradiated with visible light ($\lambda > 420$ nm) (PLS-SXE300D, Beijing Perfect Light Co. Ltd., China). Potentials of the electrode were

calibrated against the reversible hydrogen electrode (RHE) based on the following formula:

$$E_{\text{RHE}} = E_{\text{Ag/AgCl}} + 0.059\text{pH} + E^{\circ}_{\text{Ag/AgCl}} \quad (E^{\circ}_{\text{Ag/AgCl}} = 0.1976 \text{ V at } 25 \text{ }^{\circ}\text{C}) \quad (2)$$

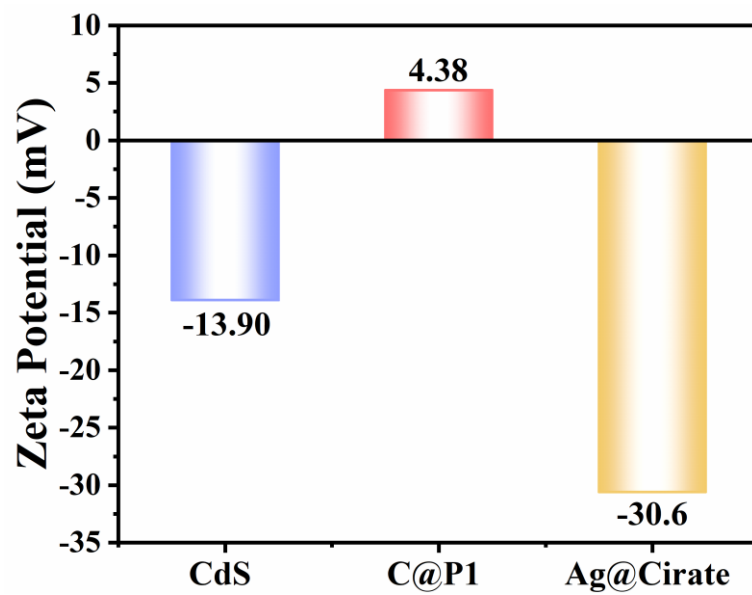


Figure S1. Zeta potentials (ξ) of CdS, C@P1 and Ag@cirate NCs.

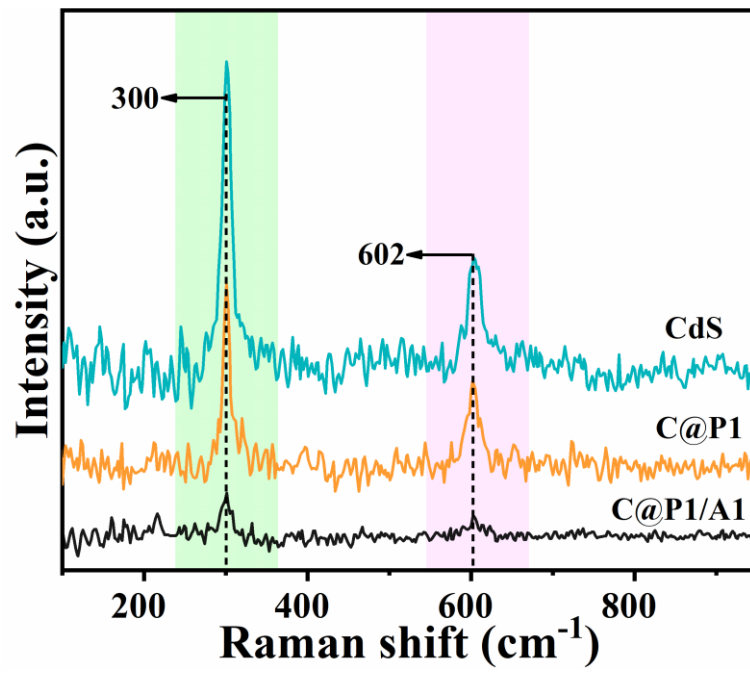


Figure S2. Raman of CdS, C@P1 and C@P1@A1 heterostructure.

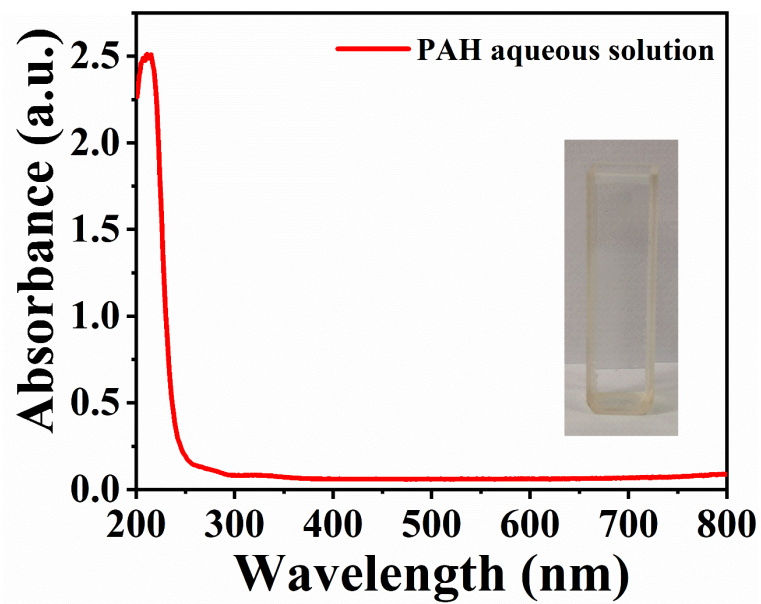


Figure S3. UV-vis absorption spectrum of PAH aqueous solution with photograph in the inset.

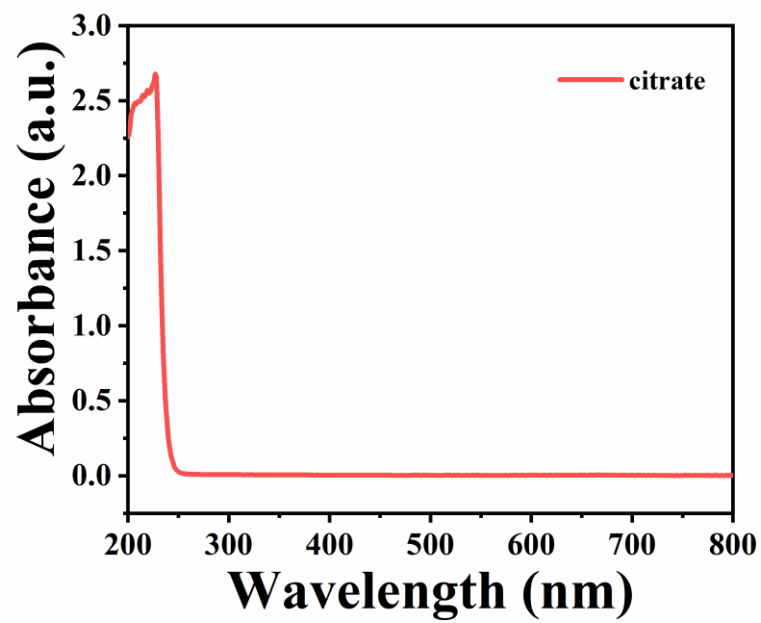


Figure S4. UV-vis absorption spectra of citrate.

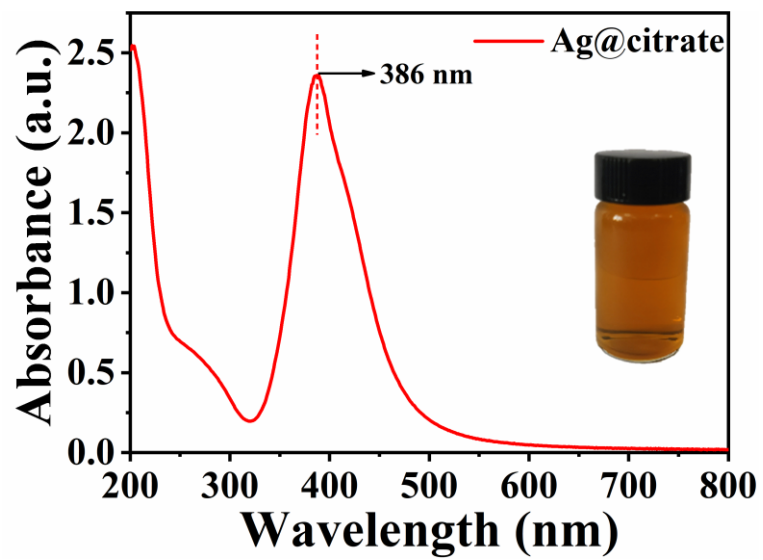


Figure S5. UV-vis absorption spectrum of Ag@citrate aqueous solution with photograph in the inset.

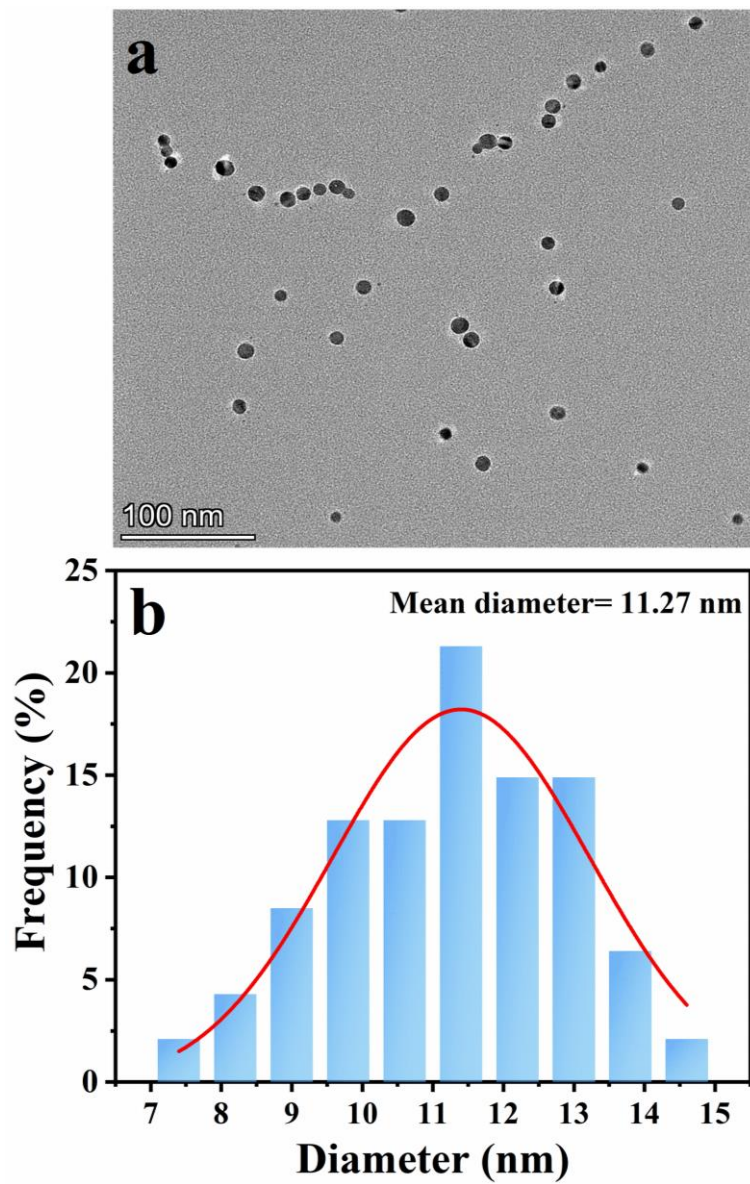


Figure S6. (a) HRTEM image of Ag@citrate NCs with (b) size distribution histogram.

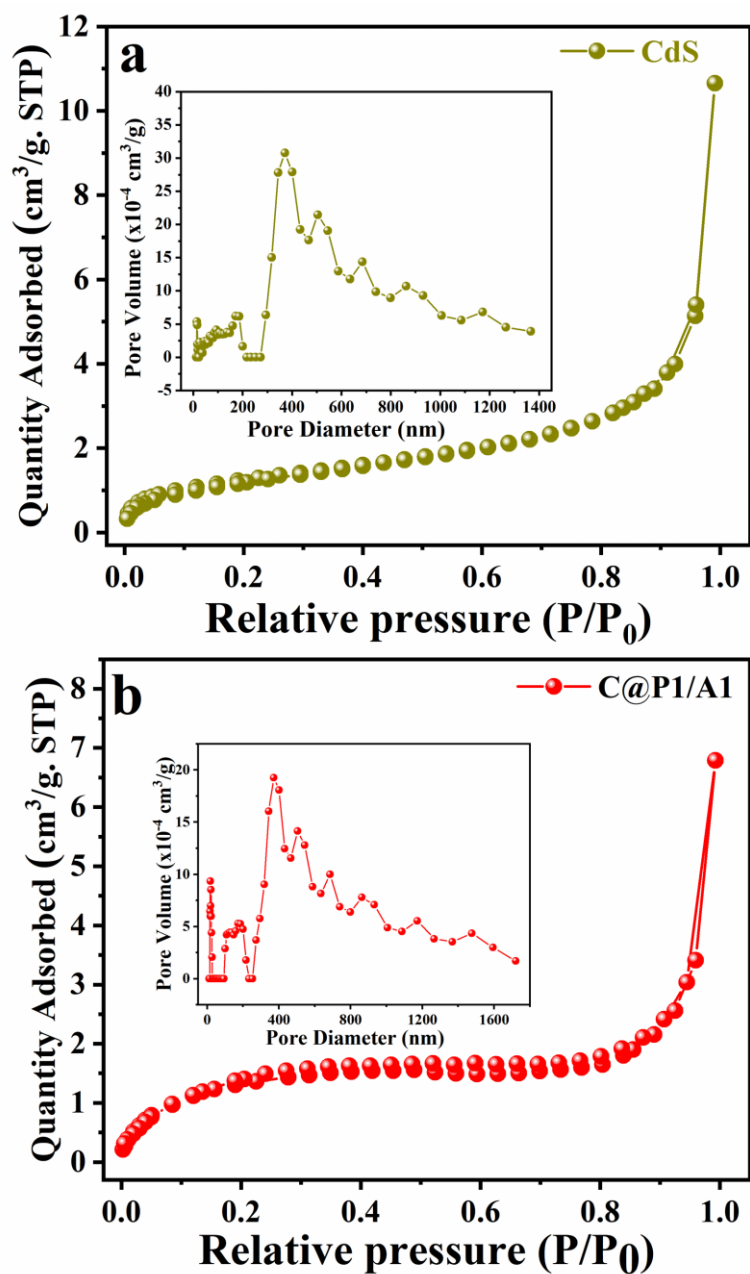


Figure S7. N₂ adsorption-desorption isotherms & pore size distribution curves (inset) of (a) CdS and (b) C@P1/A1 heterostructure.

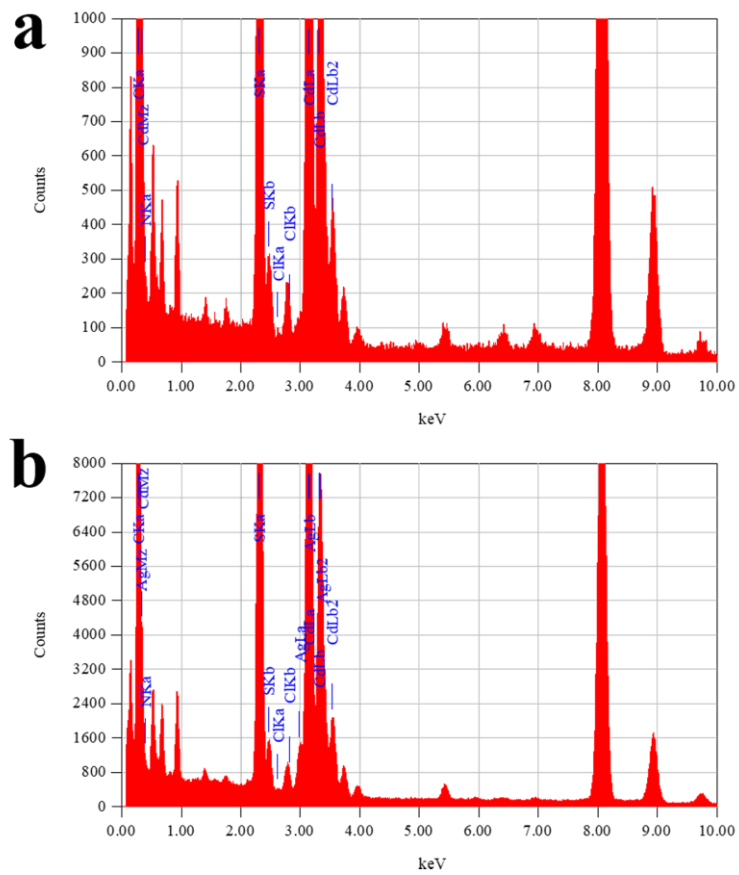


Figure S8. EDX images of (a) C@P1 and (b) C@P1@A1 heterostructure.

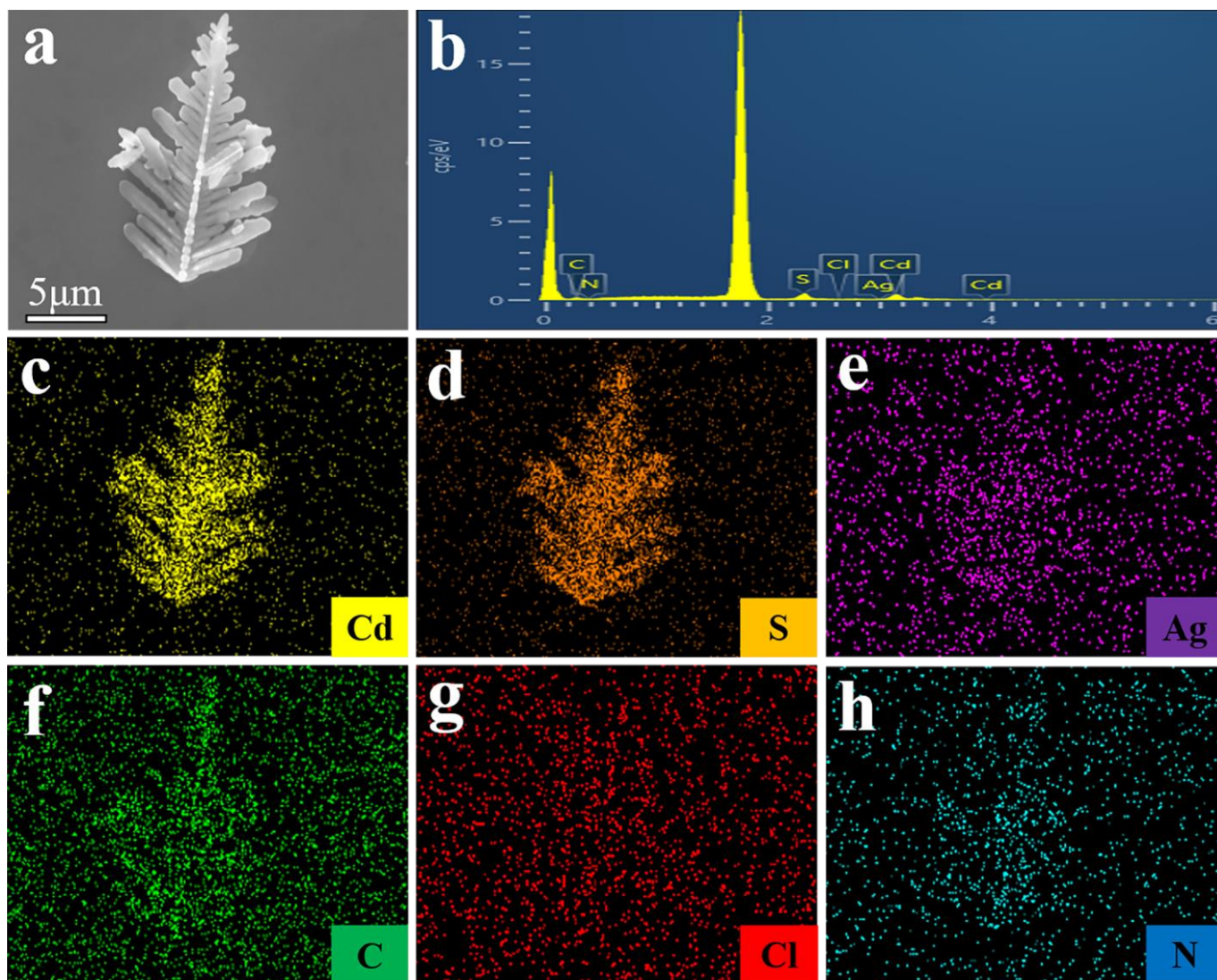


Figure S9. (a) FESEM images of C@P1/A1 heterostructure with (b) EDS and (c-h) elemental mapping results.

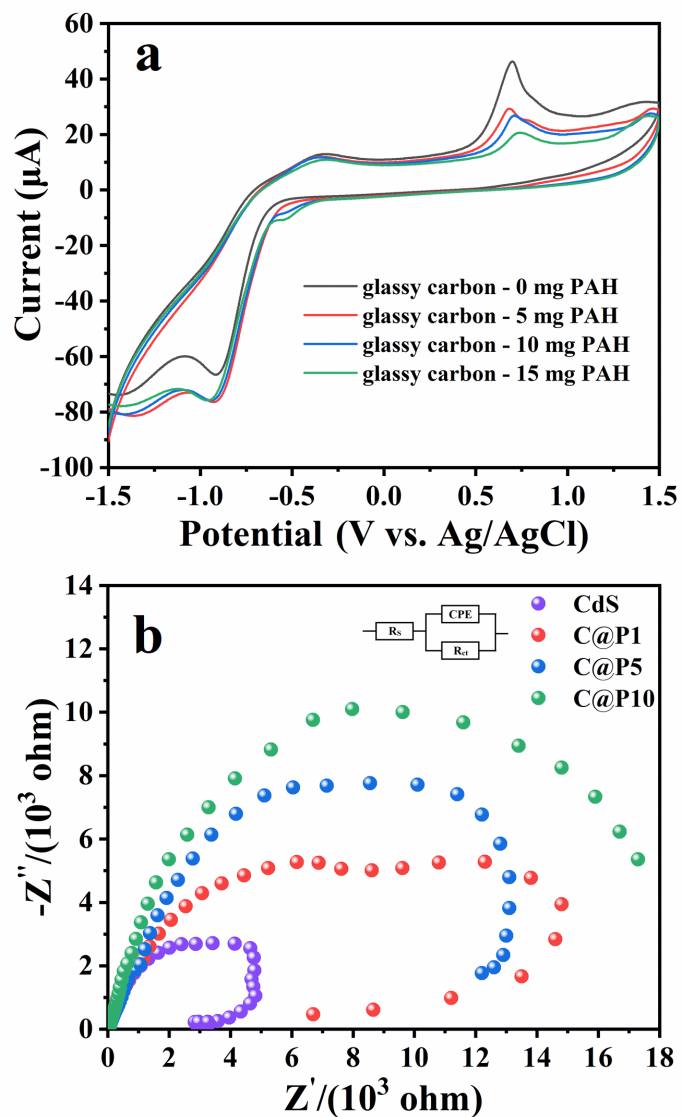


Figure S10. (a) CV curves of PAH with different addition amounts (5, 10, 15 mg) for scanning range of -1.5~1.5 V vs. Ag/AgCl. (electrolyte: degassed acetonitrile containing 0.1 M tetrabutylammonium perchlorate) and (b) EIS Nyquist plots of CdS, C@P1, C@P5 and C@P10 under visible light ($\lambda > 420 \text{ nm}$) irradiation in an aqueous Na_2SO_4 solution (0.5 M, pH = 6.69).

Note: As shown in **Figure S10a**, cyclic voltammetry (CV) curves of PAH do not show the oxidation and reduction peaks, confirming that the molecular structure of PAH does not possess the π -conjugated structure and thus suggesting that it is indeed an insulating polymer in a solid state. In the Nyquist plots of EIS results, as apparently, as the encapsulation amount of PAH increases, C@P heterostructure exhibits the larger interfacial charge transfer resistance compared with pristine CdS, which additionally confirms the generic insulating property of PAH (**Figure S10b**).

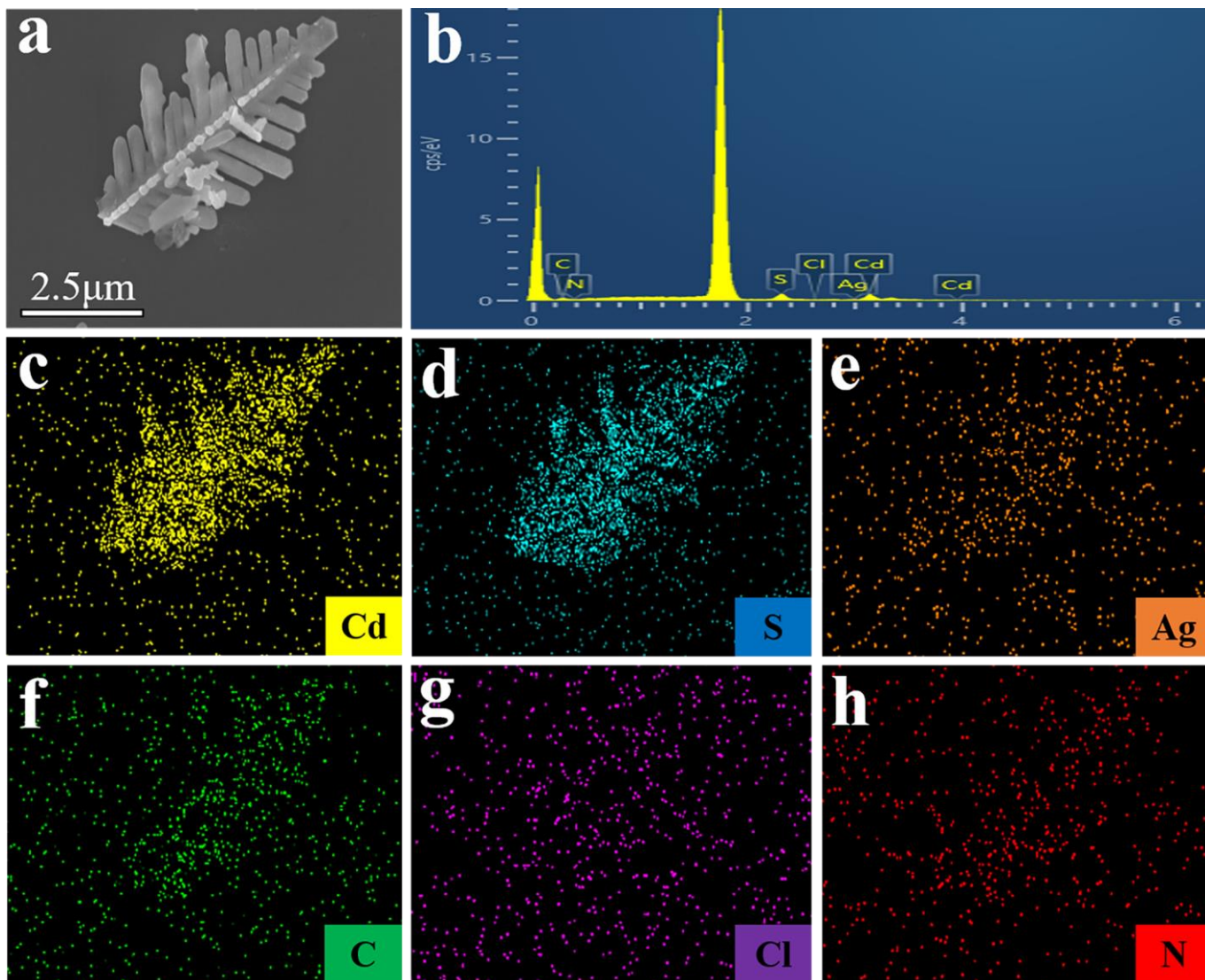


Figure S11. (a) FESEM images of C@P1/A1 heterostructure after cyclic photocatalytic CO₂ reduction with (b) EDS and (c-h) elemental mapping results.

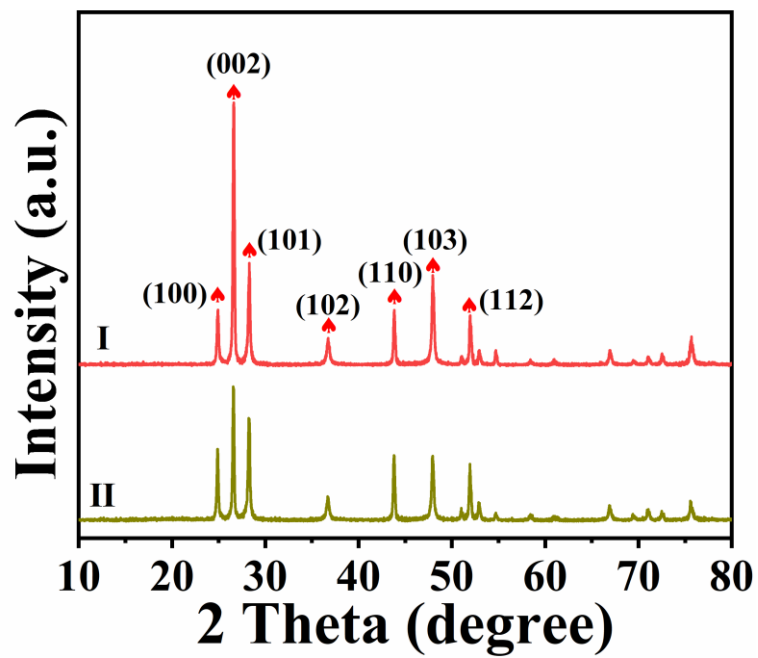


Figure S12. (a) XRD patterns of C@P1/A1 heterostructure (I) before and (II) after cyclic photocatalytic CO₂ reduction.

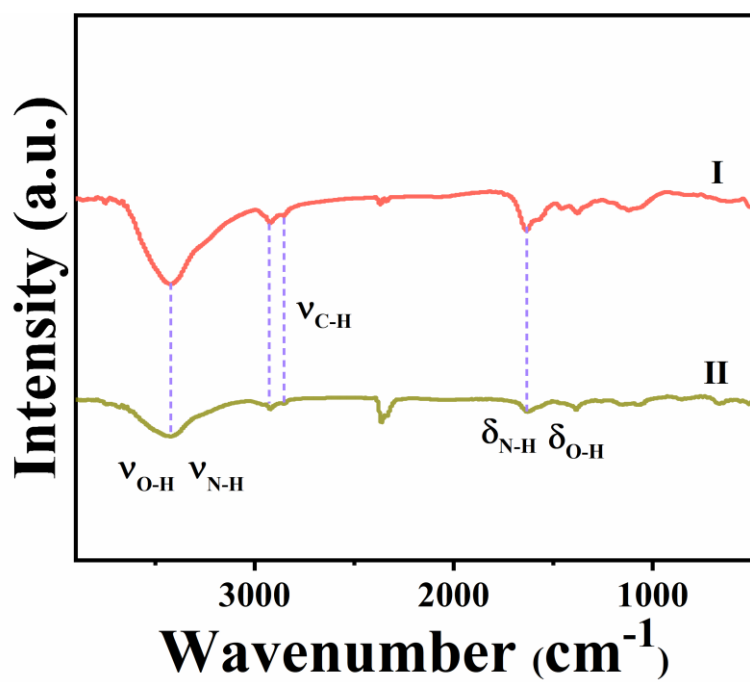


Figure S13. FTIR spectra of C@P15@Au7 heterostructure (I) before and (II) after cyclic photocatalytic CO₂ reduction.

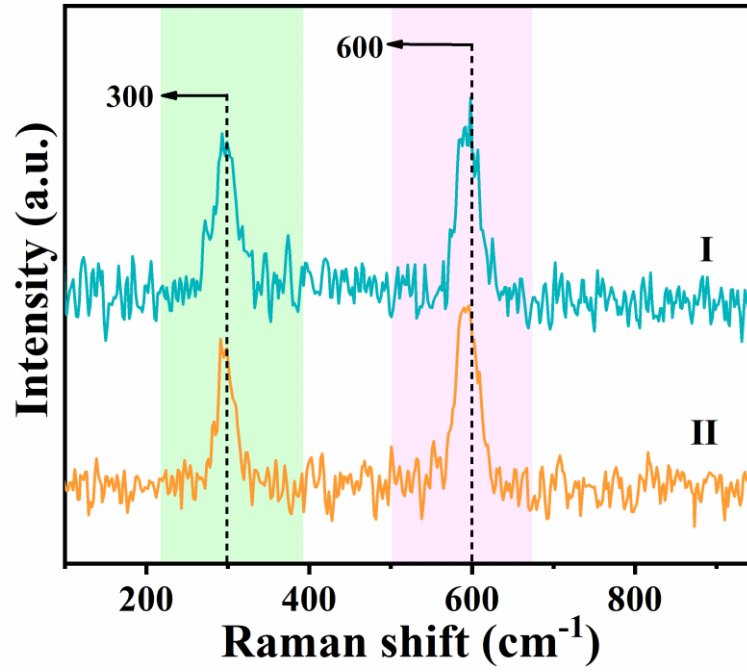


Figure S14. Raman of C@P1@A1 heterostructure (I) before and (II) after cyclic photocatalytic CO_2 reduction.

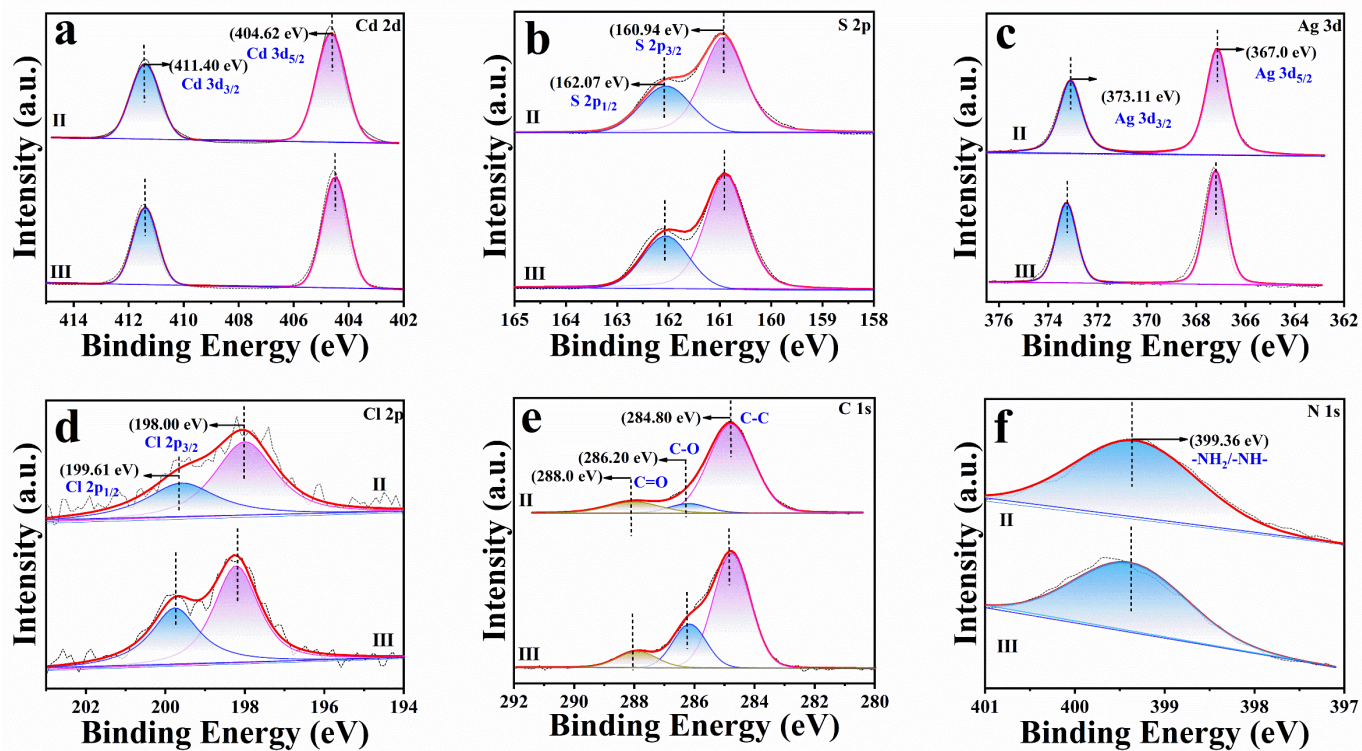


Figure S15. High-resolution (a) Cd 3d, (b) S 2p, (c) Ag 3d, (d) Cl 2p (e) C 1s and (f) N1s spectra of C@P1/A1 heterostructure (II) before and (III) after cyclic photocatalytic CO₂ reduction.

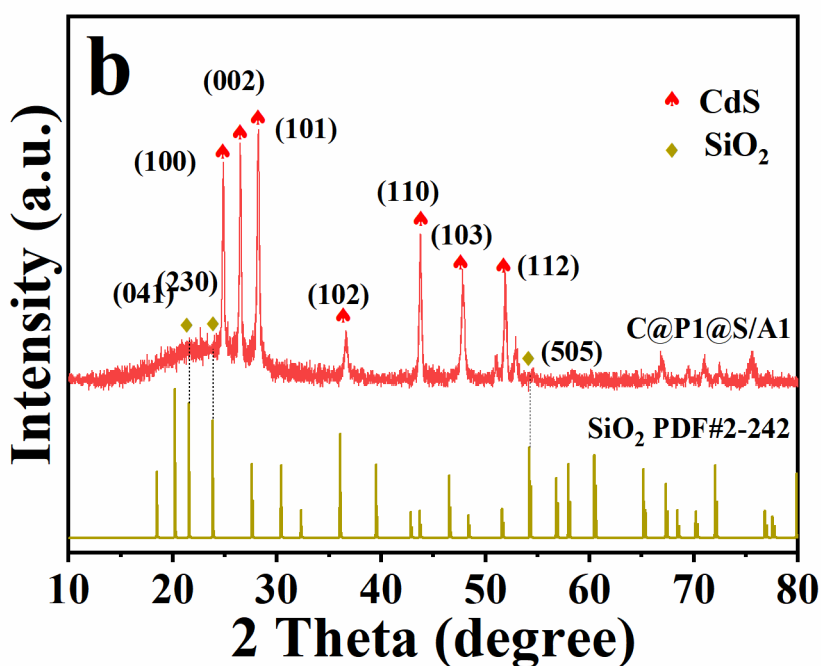
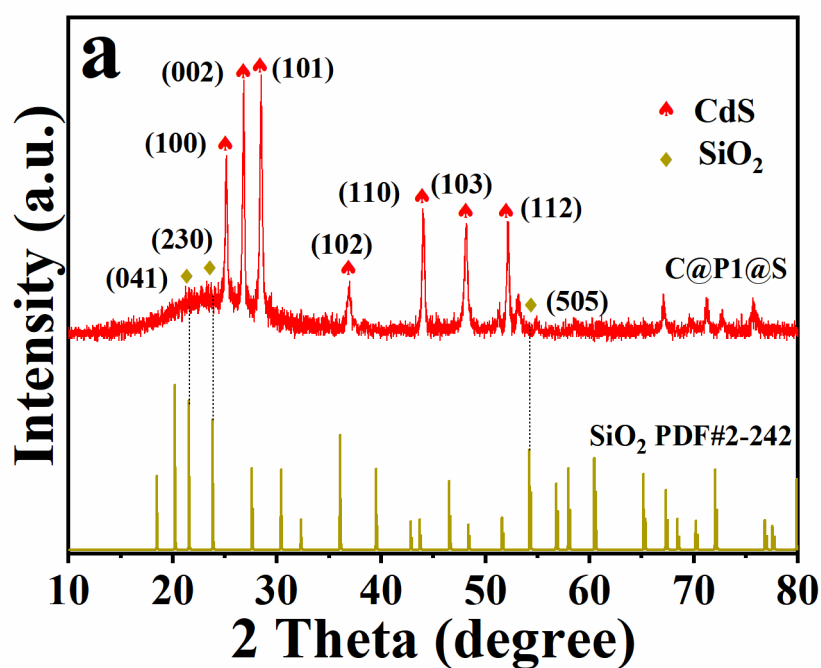


Figure S16. (a-b) XRD patterns of C@P1@S and C@P1@S/A1 heterostructures.

Note: As shown in **Figure S16**, the diffraction peaks of SiO₂ are challenging to discern due to the prominent and sharp diffraction peaks of the CdS substrate, which dominate the diffraction profile and thus obscure the faint signals of SiO₂.

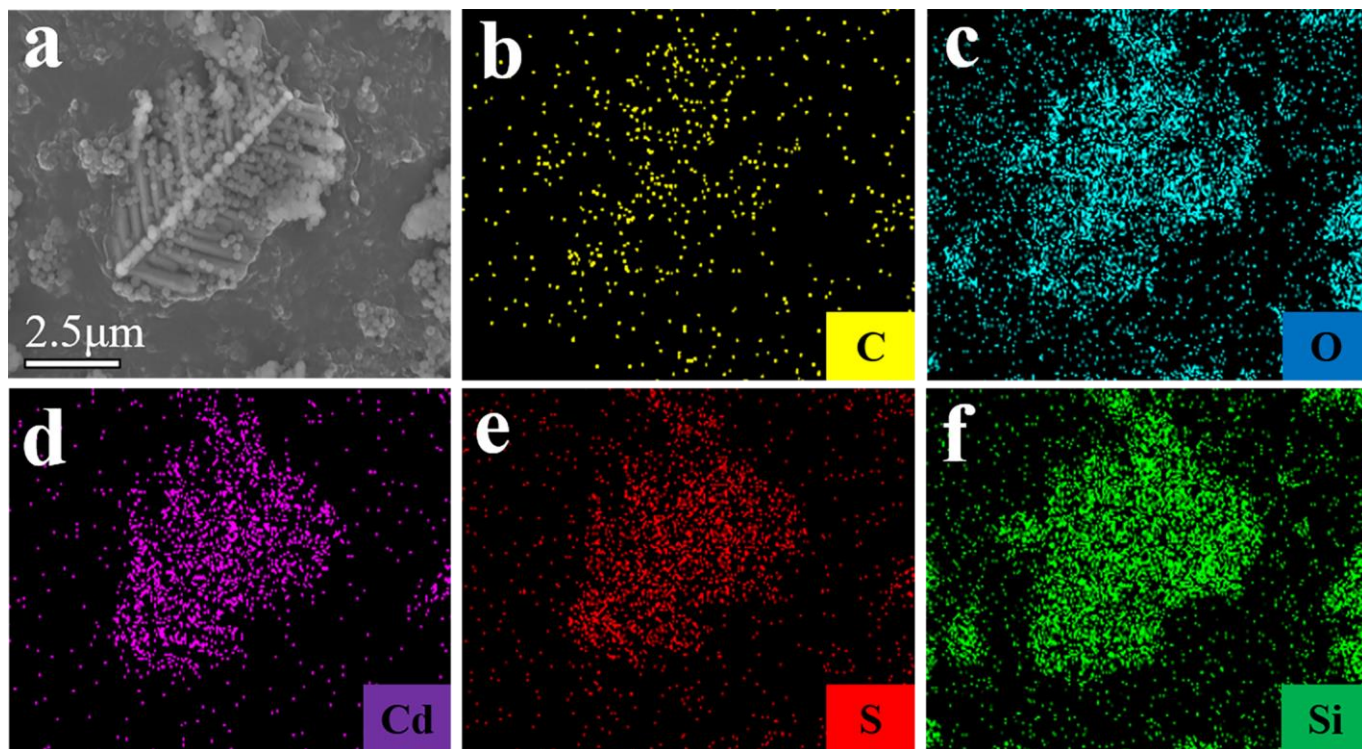


Figure S17. (a) FESEM images of C@P1@S heterostructure and (b-f) elemental mapping results.

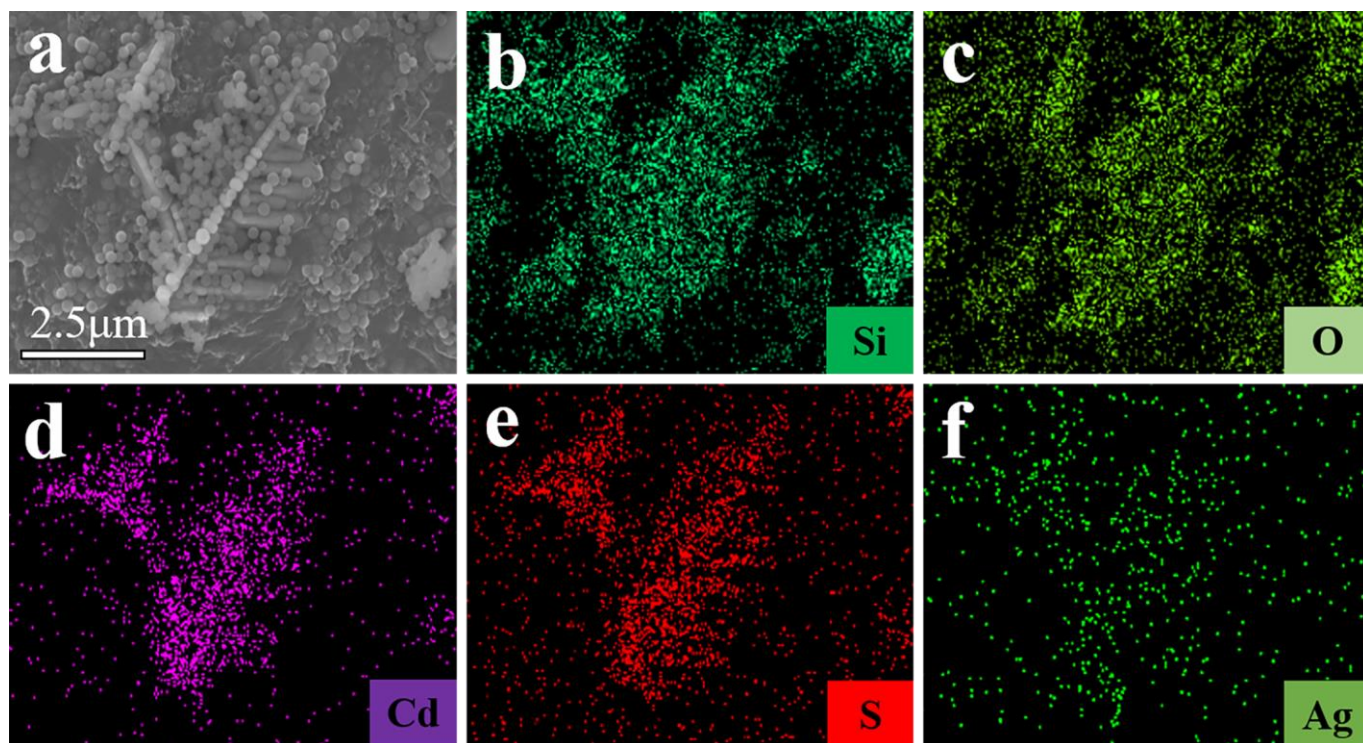


Figure S18. (a) FESEM images of C@P1@S/A1 heterostructure and (b-f) elemental mapping results.

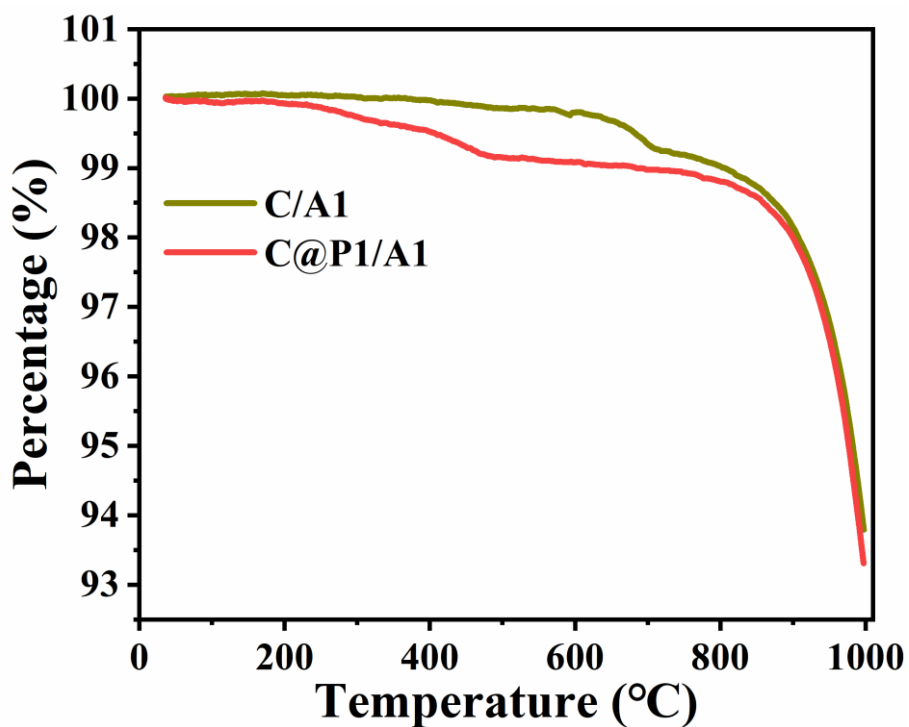


Figure S19. TGA curve of C/A1 and C@P1/A1 heterostructure.

Note: Thermogravimetric analyses for C/A1 and C@P1/A1 were conducted under nitrogen, and the results are summarized in **Figure S19**. The mass loss below 100 °C could be attributed to the removal of adsorbed water. It is noted that C@P1/A1 show a two-step thermal degradation process with 1.3 wt.% loss of PAH chains up to around 700 °C.

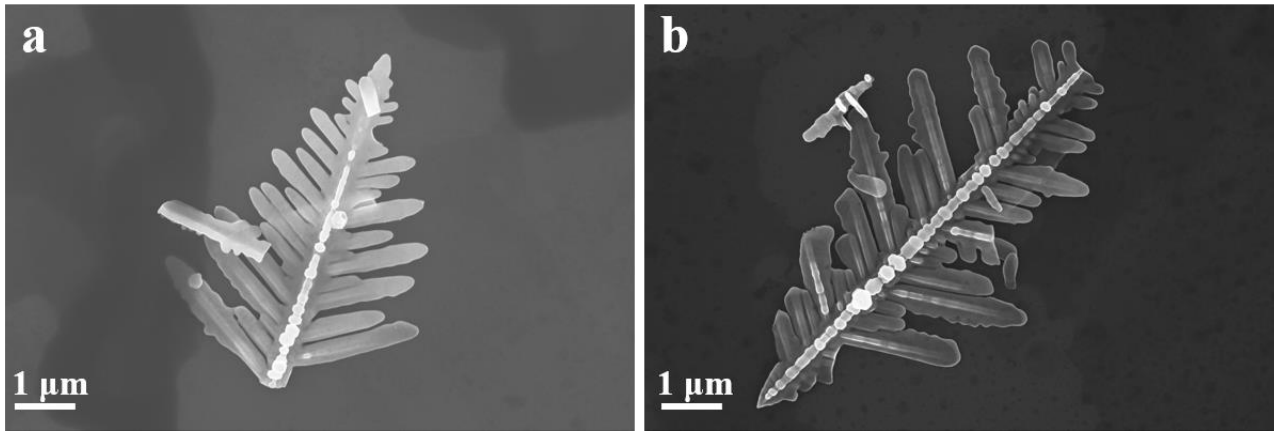


Figure S20. FESEM images of (a) C@P1/A1 and (b) C@P1/A1-700 °C.

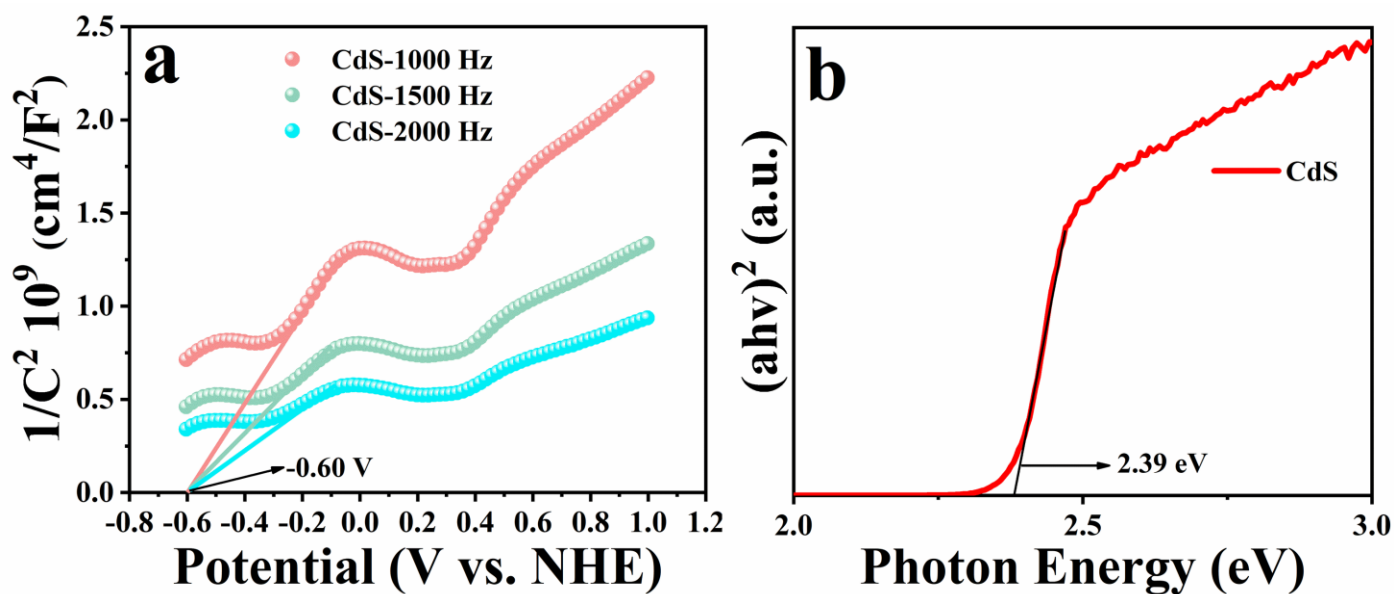


Figure S22. (a) Mott-Schottky plots of CdS along with (b) transformed plots based on the Kubelka-Munk function vs. the energy of light for CdS.

Note: According to the M-S results (**Figure S22a**), flat band potential (E_{fb}) of CdS is determined as -0.6 V vs. NHE, and considering the E_{fb} of n-type semiconductor is more positive by 0.1 V than the CB potential (E_{CB}), E_{CB} of CdS is calibrated to be -0.7 V vs. NHE. Since the band gap of CdS is 2.39 eV based on the DRS result (**Figure S22b**), valence band (VB) potential (E_{VB}) of CdS is calculated as 1.69 V vs. NHE.

Table S1. Peak position with corresponding functional group.

<i>Peak position (cm⁻¹)</i>	<i>Vibrational mode</i>	<i>Functional groups/Ingredient</i>
1665 & 3470	$\delta_{\text{O-H}}$	O-H ³
2955 & 2882	$\nu\text{-CH}_2$	CH ₂ ⁴

ν : Stretching vibration.

δ : Deformation vibration.

Table S2. Chemical bond species vs. B.E. for C@P1/A1.

<i>Element</i>	<i>CdS</i>	<i>C@P1@A1</i>	<i>Chemical Bond Species</i>
C 1s A	N.D.	284.8	C-C ⁵
C 1s B	N.D.	286.2	C-O ⁵
C 1s B	N.D.	288.0	C=O ⁵
Cd 3d_{5/2}	405.29	404.62	Cd ²⁺ ⁶
Cd 3d_{3/2}	412.03	411.40	Cd ²⁺ ⁶
S 2p_{3/2}	161.67	160.94	S ²⁻ ⁷
S 2p_{1/2}	162.83	162.07	S ²⁻ ⁷
Ag 3d_{5/2}	N.D.	367.0	Ag ⁺ ⁸
Ag 3d_{3/2}	N.D.	373.11	Ag ⁰ ⁸
Cl 2p_{3/2}	N.D.	198.0	Cl ⁻ ⁹
Cl 2p_{1/2}	N.D.	199.61	Cl ⁻ ⁹
N 1s	N.D.	399.36	-NH ₂ - ¹⁰

N.D.: Not Detected.

Table S3. Summary of specific surface area, pore volume and pore size of CdS and C@P1/A1.

<i>Samples</i>	<i>S_{BET} (m² g⁻¹)^a</i>	<i>Total pore volume (cm³ g⁻¹)^b</i>	<i>Average pore size (nm)^c</i>
CdS	4.325	0.006	65.483
C@P1/A1	3.587	0.006	72.140

^a BET surface area is calculated from the linear part of BET plot.

^b Single point total pore volume of the pores at P/P₀ = 0.95.

^c Adsorption average pore width (4V/A by BET).

Table S4. Fitted EIS results of different samples under visible light irradiation based on the equivalent circuit

<i>Samples</i>	<i>R_s/ohm</i>	<i>R_{ct}/ohm</i>	<i>CPE /(F·cm⁻²)</i>
C/A1	4.678	19510	2.892E-5
C@P1/A1	14.87	5159	4.229E-5

Note: As shown in **Table S4**, R_{ct} values were obtained by fitting the EIS results according to a simple equivalent circuit composed of a series of resistance (**Figure 5c**, inset). Apparently, C@P1@A1 demonstrates the smallest R_{ct} value in comparison with other counterparts, indicative its lowest interfacial charge transfer resistance.

Table S5. Photoactivities of C/A1 and C@P1/A1 towards selective reduction of aromatic nitro compounds to amino derivatives under visible light irradiation ($\lambda > 420$ nm).

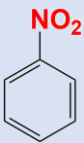
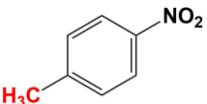
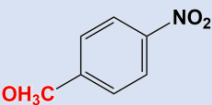
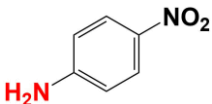
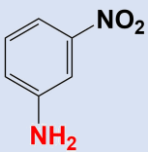

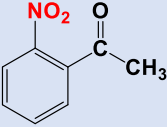
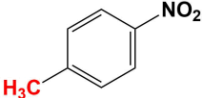
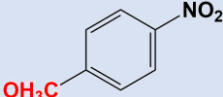
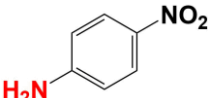
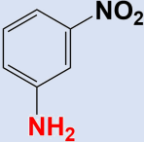
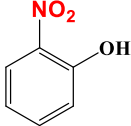
<i>Substrate</i>	<i>Samples</i>	<i>Conversion (%)</i>
	C/A1	45.92
	C@P1/A1	81.63
	C/A1	47.74
	C@P1/A1	86.60
	C/A1	57.37
	C@P1/A1	80.22
	C/A1	37.81
	C@P1/A1	44.16
	C/A1	22.56
	C@P1/A1	30.84
	C/A1	25.06
	C@P1/A1	35.05

Table S6. Photoactivities of C@P1@S/A1, C@P1/A1-700 °C and C@P1/A1 towards selective reduction of aromatic nitro compounds to amino derivatives under visible light irradiation ($\lambda > 420$ nm).

<i>Substrate</i>	<i>Samples</i>	<i>Conversion (%)</i>
	C@P1@S/A1	6.58
	C@P1/A1-700 °C	13.32
	C@P1/A1	35.05
	C@P1@S/A1	24.46
	C@P1/A1-700 °C	44.35
	C@P1/A1	86.63
	C@P1@S/A1	11.28
	C@P1/A1-700 °C	25.36
	C@P1/A1	80.22
	C@P1@S/A1	8.15
	C@P1/A1-700 °C	3.46
	C@P1/A1	44.16
	C@P1@S/A1	6.46
	C@P1/A1-700 °C	11.88
	C@P1/A1	30.84
	C@P1@S/A1	18.88
	C@P1/A1-700 °C	22.03
	C@P1/A1	34.18

References

- (1) Li, C.; Han, L.; Liu, R.; Li, H.; Zhang, S.; Zhang, G. Controlled synthesis of CdS micro/nano leaves with (0001) facets exposed: enhanced photocatalytic activity toward hydrogen evolution. *J. Mater. Chem.* **2012**, *22*, 23815-23820.
- (2) Xiao, F.-C. Layer-by-Layer Self-Assembly Construction of Highly Ordered Metal-TiO₂ Nanotube Arrays Heterostructures (M/TNTs, M = Au, Ag, Pt) with Tunable Catalytic Activities. *J. Phys. Chem. C* **2012**, *116*, 16487-16498.
- (3) Xu, S.; Lin, H.-J.; Lin, X.; Fu, X.-Y.; Hou, S.; Wei, Z.-Q.; Mo, Q.-L.; Xiao, F.-X. Intercalating ultrathin polymer interim layer for charge transfer cascade towards solar-powered selective organic transformation. *J. Catal.* **2021**, *399*, 150-161.
- (4) Zhang, Q.; An, Q.; Luan, X.; Huang, H.; Li, X.; Meng, Z.; Tong, W.; Chen, X.; Chu, P. K.; Zhang, Y. Achieving significantly enhanced visible-light photocatalytic efficiency using a polyelectrolyte: the composites of exfoliated titania nanosheets, graphene, and poly(diallyl-dimethyl-ammonium chloride). *Nanoscale* **2015**, *7*, 14002-14009.
- (5) Dai, X.-C.; Huang, M.-H.; Li, Y.-B.; Li, T.; Hou, S.; Wei, Z.-Q.; Xiao, F.-X. Probing the Advantageous Photosensitization Effect of Metal Nanoclusters over Plasmonic Metal Nanocrystals in Photoelectrochemical Water Splitting. *J. Phys. Chem. C* **2020**, *124*, 4989-4998.
- (6) Rengaraj, S.; Venkataraj, S.; Jee, S. H.; Kim, Y.; Tai, C. W.; Repo, E.; Koistinen, A.; Ferancova, A.; Sillanpaa, M. Cauliflower-like CdS microspheres composed of nanocrystals and their physicochemical properties. *Langmuir* **2011**, *27*, 352-358.
- (7) Ojha, K.; Debnath, T.; Maity, P.; Makkar, M.; Nejati, S.; Ramanujachary, K. V.; Chowdhury, P. K.; Ghosh, H. N.; Ganguli, A. K. Exciton Separation in CdS Supraparticles upon Conjugation with Graphene Sheets. *J. Phys. Chem. C* **2017**, *121*, 6581-6588.
- (8) Liang, H.; Liu, B.-J.; Tang, B.; Zhu, S.-C.; Li, S.; Ge, X.-Z.; Li, J.-L.; Zhu, J.-R.; Xiao, F.-X. Atomically Precise Metal Nanocluster-Mediated Photocatalysis. *J. Catal.* **2022**, *12*, 4216-4226.
- (9) Zhao, S.; Zhang, Y.; Zhou, Y.; Zhang, C.; Sheng, X.; Fang, J.; Zhang, M. Reactable Polyelectrolyte-Assisted Synthesis of BiOCl with Enhanced Photocatalytic Activity. *ACS Sustainable Chem. Eng.* **2017**, *5*, 1416-1424.
- (10) Cheng, W.; Yang, C.; Ding, X.; Engler, A. C.; Hedrick, J. L.; Yang, Y. Y. Broad-Spectrum Antimicrobial/Antifouling Soft Material Coatings Using Poly(ethylenimine) as a Tailorable Scaffold. *Biomacromolecules* **2015**, *16*, 1967-1977.